HanGuenesBaeKimChaeShinChoiPribatLee2011

NANO LETTERS

LETTER

pubs.acs.org/NanoLett

Influence of Copper Morphology in Forming Nucleation Seeds for Graphene Growth

Gang Hee Han,[†] Fethullah Güneş,[†,‡] Jung Jun Bae,[†] Eun Sung Kim,[†] Seung Jin Chae,[†] Hyeon-Jin Shin,[‡] Jae-Young Choi,[‡] Didier Pribat,[†] and Young Hee Lee*[,†]

[†]BK21 Physics Division, WCU Department of Energy Science, Center for Nanotubes and Nanostructured Composites, and Sungkyunkwan Advanced Institute of Nanotechnology and [‡]Graphene Center, Samsung Advanced Institute of Technology, Sungkyunkwan University, Suwon 440-746, Korea

Supporting Information

ABSTRACT: We report that highly crystalline graphene can be obtained from well-controlled surface morphology of the copper substrate. Flat copper surface was prepared by using a chemical mechanical polishing method. At early growth stage, the density of graphene nucleation seeds from polished Cu film was much lower and the domain sizes of graphene flakes were larger than those from unpolished Cu film. At later growth stage, these domains were stitched together to form monolayer graphene, where the orientation of each domain crystal was unexpectedly not much different from each other. We also found that grain boundaries and intentionally formed scratched area play an important role for nucleation seeds. Although the best monolayer graphene was grown from polished Cu with a low sheet resistance of 260 Ω/sq, a small portion of multilayers were also formed near the impurity particles or locally protruded parts.

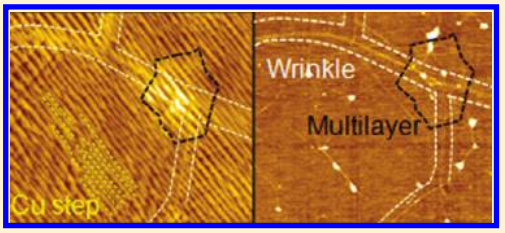

KEYWORDS: Graphene, Chemical vapor deposition, Seed, Copper, Wrinkle

Unlike graphene synthesis on nickel using chemical vapor deposition (CVD),[1−6] graphene synthesis on copper has been useful particularly for monolayer formation because of low carbon solubility in copper.[7] The growth mechanism in latter case is dominated by "surface adsorption" rather than bulk diffusion due to short diffusion length.[8,9] Several growth factors have been modified for improving graphene quality such as growth temperature, gas feeding ratio, and pressure.[10,11] Nevertheless, the obtained graphene crystallinity and electrical conductivity are still far from those of highly oriented pyrolytic graphite (HOPG) and theoretical limit.[12] More importantly, origin of formation of nucleation seeds, multilayer formation, and wrinkle formation remains unanswered. Here, we report that morphology of copper surface such as roughness, grain boundary, defects, and impurity particles plays a crucial role for forming nucleation seeds of monolayer and multilayer graphene. The formation of nucleation seeds was controlled by the chemical mechanical polishing (CMP) and scratching, which led to change the density of nucleation seeds and growth rate. The polarized confocal Raman spectroscopy demonstrates that the obtained graphene that is stitched from several graphene flakes has similar orientation to each other. We further found out that bumpy copper surface induces wrinkle formation.

To synthesize graphene, Cu foil purchased from Nilaco (Lot No. 113321, 99.96%, 100 μm in thickness) was chemically and mechanically polished (Supporting Information S1). To clarify the effect of the roughness, graphene was simultaneously grown on unpolished and polished Cu foil using atmospheric pressure chemical vapor deposition (APCVD). Figure 1a and 1b are the transferred graphene onto silicon oxide (300 nm)/silicon (500 μm) substrate from polished and unpolished foil, respectively. Because the ratio of carbon source to hydrogen and argon gas is relatively high (0.5%) compared with other groups (few tens of ppm or less),[13,14] growth rate (~3 μm/sec) is higher than the previous results. Graphene was nearly fully covered on both copper surfaces after 10 s. The obtained graphene was transferred onto Si/SiO_2 wafer by poly(methyl methacrylate) (PMMA) layer. At the early growth stage of 3 s, small domain graphenes were nucleated randomly over the polished sample with an average domain size of formed ~140 μm^2, which is in good contrast with a small average domain size of about ~30 μm^2 in the unpolished sample (top panels of Figure 1a and 1b). On the other hand, the number density of graphene domains was 5.5×10^3 ea/mm^2 in the polished sample, much smaller than 2.4×10^4 ea/mm^2 in the unpolished sample. In other words, abundant nucleation seeds are available on the unpolished sample, although their growth rate is rather slower than that of polished sample. Rough surface or impurities existing on the unpolished sample may act as nucleation seeds. It is intriguing to see that every domain has small (dark) dot near the center, which may act as a nucleation seed. This will be discussed later.

With increasing growth time (5 s), the number of graphene domains was reduced in both cases by coalescing small grains into large ones. Nearly 70−80% of copper surfaces were covered

Received: June 13, 2011
Revised: August 6, 2011
Published: August 24, 2011

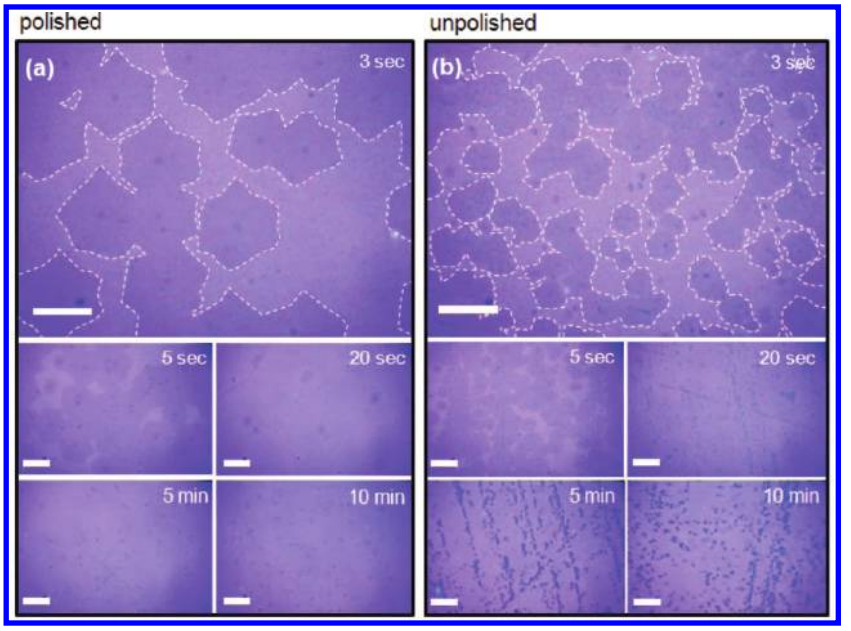

Figure 1. Optical micrographs of graphene flakes grown by (a) polished and (b) unpolished Cu substrate at early growth stage and the corresponding time evolutions in the bottom panel in which graphene was transferred onto SiO_2/Si wafer. Multilayer islands were developed on unpolished Cu foil as the growth time increased. Size of the scale bar is 10 μm.

and the full coverage of monolayer was obtained in 10 s in both cases. At 20 s, the monolayer graphene was still retained on the polished sample, while multilayer stripelike islands of graphene started to appear in the unpolished sample. The multilayer stripelike islands[7] were thicker and clearly visible in the unpolished sample at longer times of 5 and 10 min. These multilayer stripes were originated from the surface morphology of the unpolished copper. The monolayer graphene was formed initially on the copper stripes. This monolayer graphene could be strained due to the curvature of copper stripes to increase adsorption energy for the incoming carbon atoms and thus act as nucleation seeds to form the stripe-like multilayer graphene. On the polished sample, monolayer graphene was retained and no multilayer stripes were formed even at longer growth time, revealing the self-limiting growth condition. The higher number density in the unpolished sample (Figure 1b) results from the pre-existing (impurity) particles and rough copper surface that are more likely to be abundant in the unpolished Cu surface. Atomic force microscopy (AFM) image also shows clearly the multilayer formation near the particles (Supporting Information S2). The best sample quality was obtained from the CVD-grown sample with CMP-treated Cu film after 15 min growth. The sheet resistance of graphene transferred to SiO_2 substrate was 260 Ω/sq, exceeding the reported values.[15]

To elucidate morphology dependence more clearly, the graphene growth near the grain boundary and the scratched area was further investigated. The scanning electron microscopy (SEM) image shows grain boundary of copper surface (yellow arrows, left panel) and scratched area (red arrows, right panel) in Figure 2a−c. It is interesting to see that the number density of nucleation seeds is larger near the grain boundary compared to the remote areas away from the boundary and furthermore the graphene flakes were formed near the line of Cu grain boundary not on the grain boundary. Since the carbon solubility in Cu is low, it is unlikely that carbon atoms can be out-diffused from the line of grain boundary in the case of Ni.[16] Similar phenomenon was also observed near the scratched area. No other impurities were involved in growing graphene flakes near the scratched area, since the same Cu foil was used to create scratches. Cu particles were formed along the scratched line during preheating stage of growth and acted as nucleation seeds, as shown in the schematic of Figure 2d.

Multilayer formation around the nanoparticles was clearly visible from AFM and SEM images, as shown in Figure 3a,b. Interestingly, nanoparticles were consistently located in the middle of the graphene domains at early growth stage. This strongly implies that nanoparticles act as nucleation seeds for graphene growth. During CMP, alumina nanoparticles remained on Cu surface, which was confirmed by SEM energy-dispersive X-ray spectroscopy (EDX) data (Supporting Information S3). After transfer of the graphene onto SiO_2/Si wafer (see also Supporting Information S3), Raman signals (WiTec, 532 nm) were obtained from a few positions (Figure 3c). Bilayer graphene was formed near the nanoparticles, while monolayer graphene was formed away from the nanoparticles, as confirmed from G′/G intensity ratio. No appreciable D band (D/G intensity ratio is less than 0.1) was observed in monolayer region, while D-band (ratio is ∼1.0) was developed at the edge of the graphene domains.

The shape of domains becomes rather arbitrary at early stage, as shown above. Initially the domain shapes are typically hexagonal. Figure 3d shows optical images of single domain (upper panel) and bidomain (lower panel), where two domains are stitched to each other. The next panels show the related confocal Raman mappings of D-band. No appreciable D-band (D/G ratio is less than 0.1) was observed throughout the domain except edge area. Bright background outside domain indicates the presence of amorphous carbons introduced during growth. To elucidate the presence of defects or strained area more clearly, these samples were mildly oxidized for 30 min at ∼400 °C and further oxidized in situ several times. After 1 h air oxidation, amorphous carbons

dx.doi.org/10.1021/nl201980p |*Nano Lett.* 2011, 11, 4144–4148

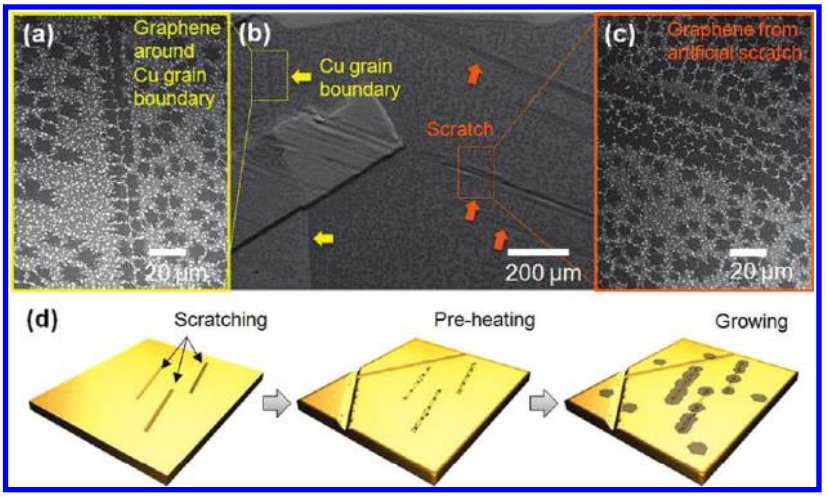

Figure 2. SEM images of initial formation of graphene flakes grown near Cu grain boundaries and scratched area in different magnifications for 5 s (a−c). (d) The schematics of the scratched surface morphology and the related graphene flake formation (gray).

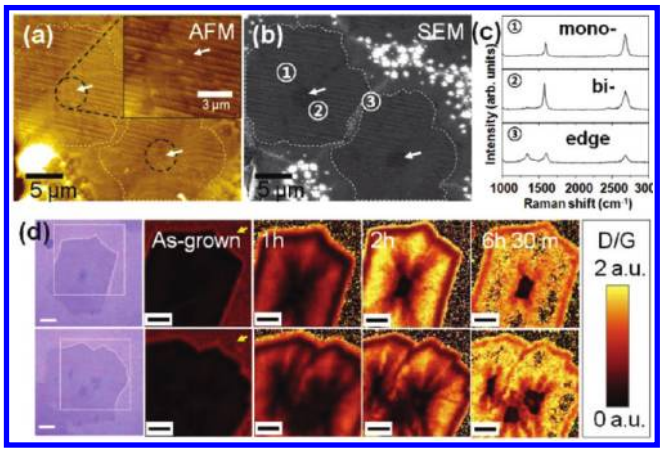

Figure 3. (a,b) AFM and SEM images of graphene flakes which was grown for 5 s on Cu substrate with CMP treatment. At the center of flakes, impurity nanoparticles were acted as seeds of monolayer and bilayer graphene. (c) Raman signal (excitation wavelength 532 nm) from mono-, bi- and edge of graphene. D-band signal was enhanced at the edge of flakes. (d) The oxidized graphene in air around 400 °C. D-band and G-band were mapped to calculate D/G ratio in the range of 1300−1400 and 1575−1615 cm^{-1}, respectively. The scale bar is 3 μm.

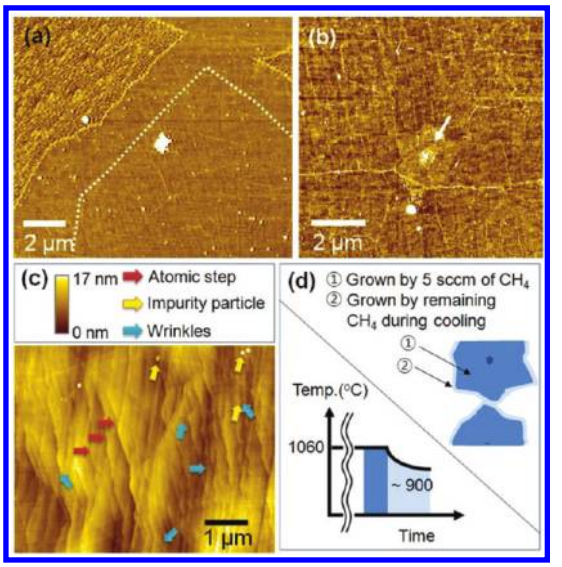

Figure 4. (a) AFM image of the transferred graphene flakes onto Si/SiO_2 substrate. Different graphene quality near the edge of graphene flake distinguished by the dotted lines. (b) AFM image of graphene layer inside the dotted line of (a). The white arrow indicates the presence of nanoparticle and nearby multilayer flake. (c) Various structures: Cu atomic steps (red arrow), impurity particles (yellow arrow), and wrinkles of graphene (blue arrow), which can influence on graphene growth. (d) Schematic for graphene flake growth. Graphene flake was grown for 5 s (①). After growth, during cooling step (without gas feeding), the remaining gas induced additional growth (②). Growth temperature was 1060 °C for step ① and graphene can be grown further until the temperature is cooled down to around 900 °C.

were completely removed outside the domain boundary. The outermost edge became bright due to preferable oxidation. More importantly, D-band with flakes was enhanced in a rather unexpected way, that is, the multilayer region near the center remained unchanged, while the region away from the center developed relatively large D-band in a fanlike pattern. This pattern is similar to the previous report that multiorientational domains centered in the nucleation seed are formed radially from the CVD-grown sample.[14]

On the other hand, the most stable stripe is formed along the edge. This trend of oxidation was persistently maintained with the similar edge frame at long oxidation times even until some portion of the inner graphene was oxidized away. It is rather surprising to see from the bottom panel that the stitched boundary of two domains as indicated by the dark line in the middle remained unchanged, in other words, very stable, together with multilayer portion in the middle until the last moment of oxidation even after 6.5 h. High stability of the domain boundary may originate from the annealing effect during stitching process of CVD growth at high temperature. Pentagons and heptagons that are formed easily at the boundary could be transformed into hexagons by catalytic reaction with additional supply of carbon atoms.

Figure 4a,b shows AFM images of graphene after transfer to SiO_2/Si substrate. The surface morphology of the edge ribbon indicated by the dotted line with a width of 1−2 μm (in Figure 4a) is rather clean and flat, whereas the inner portion of

dx.doi.org/10.1021/nl201980p |*Nano Lett.* 2011, 11, 4144–4148

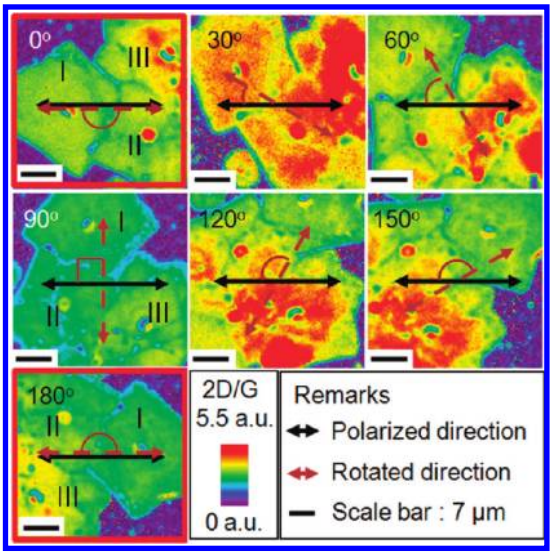

Figure 5. Polarized Raman spectroscopy (laser excitation wavelength, 532 nm) was performed in the range of 0 to 180° with an interval of 30°. Black arrows and dashed red arrows indicate polarization direction of light and rotation angle of sample. The peak intensity was decreased about ~20% after 7 times of mapping (the difference between 0 and 180°).

domains remained cracked, as clearly observed from the high-resolution AFM image in Figure 4b. These streaks actually came from the stepped copper surface, as shown in Figure 4c. Graphene grows following the corrugated stepped Cu surface. The corrugated graphene can be preserved after transfer, creating such streaks shown in Figure 4b. The strain-relaxation may occur in many different ways. For instance, one consequence of the strain release is the formation of wrinkles (see also Supporting Information S4). These are the sources of fast oxidative etching shown in Figure 3d particularly in the inner region. The clean surface morphology near the edge ribbon is rather peculiar. The growth temperature in our case was 1060 °C near the Cu melting temperature (~1080 °C). The surface of Cu foil is nearly melting. Upon cooling with a termination of carbon source, Cu foil shrinks and creates heavy thermal stress on the grown graphene to leave wrinkles and extra stress. On the other hand, graphene can be further cloned at the edge of graphene flakes by the residual carbon gases until the temperature reaches some critical value where graphene is no longer formed (Figure 4d). During this extra cloning process of graphene, copper substrate is cooled down as well so that the thermal expansion of Cu foil is severely reduced. As a consequence, formation of the streaks and wrinkles is minimized, leading to a rather clean graphene surface.

It has been reported that the intensity of 2D-band of HOPG graphene is changed upon polarization of the incident light.[18−20] Since the graphene grown by CVD is composed of multiple domains stitched with each other, it will be intriguing to see the polarization dependence of our CVD-grown sample. Our sample is composed of three domains indicated by the domain boundary at different colors (I, II, III), as shown in the confocal Raman mapping of 2D/G intensity ratio in Figure 5. G-band and 2D-band were mapped in the range of 1575−1615 and 2660−2725 cm^{-1}, respectively. The domain boundary lines are visible perhaps due to the incomplete annealing by the short growth time. Colors of domains are similar to each other, although one domain in the top-right position has stronger 2D intensity than other domains. This implies that the orientations of each domain are not much different from each other. By rotating an angle of sample by 30°, a periodic repetition of colors is observed with 180° rotation that has been reported as a sinusoidal function, that is, at 180°, the intensity was similar to that at 0°. The absolute intensity at 180° was suppressed about 20% compared to zero degree due to the possible mild oxidation of graphene layer induced by laser irradiation.[21,22] The intensity variance inside each domain was not appreciable, indicating uniformity of the graphene crystallinity. While two domains (I and II) showed similar 2D/G intensity ratio, the domain III revealed higher 2D intensity, indicating higher crystal quality. One intriguing observation is that three domains exhibited maximum and minimum intensities in phase with different orientations. This indicates that three domains may have the similar orientational ordering. This is in good contrast with the previous report that initial hexagonal domains have different orientations.[17,23] The coincidental observation is remarkable, because each domain meets with random orientation and stitches together to form one piece of large size graphene. Several other flakes have been observed with similar manner (Supporting Information, S5). This implies that each graphene domain may grow with a preferred orientation. The correlation of domain direction may be related to the polishing conditions where well-defined steps are formed to a preferential direction. The reason how the similar orientation of graphene is retained is not clear at this moment. This requires further study. The best sheet resistance obtained using APCVD with polished Cu foil was 260 ohm/sq.

In summary, we have studied influences of copper morphology for the formation of nucleation seeds during initial graphene growth stage. The number of nucleation seeds and graphene domain sizes (growth rate) were strongly dependent on whether copper substrate is polished or not. Impurity particles, Cu particles, or alumina particles introduced during polishing can also play a crucial role for nucleation of graphene, which is the origin of small coverage of multilayer region. We further found that artificial scratches and grain boundary can also act as nucleation seeds. We expect that our approach can provide a beneficial influence to improve the quality of graphene in future research.

Experimental Section. *Synthesis of Graphene.* A 100 μm thick copper foil (from Nilaco, 99.96%) was used for graphene growth in APCVD. The temperature of the chamber was heated up to 1060 °C with 1000 sccm of Ar and 200 sccm of H_2 and annealed for 20 min. For growth, H_2 gas was reduced to 10 and 3 sccm of methane gas was injected. After growth the sample was cooled down to room temperature. The detail cooling rate has been described elsewhere.[4]

Transfer Process of a Graphene. PMMA (e-beam resist, 950 k C4, Microchem) was spin-coated on the graphene/Cu foil at 1000 rpm for 60 s. To etch Cu foil, the sample was submerged in copper etchant (CE-100, Transene) for ~30 min. After rinsing by deionized water for a few times, PMMA/graphene layer was fished onto SiO_2 (300 nm)/Si wafer and PMMA was removed by acetone later.

Measurements. For optical photo images and confocal Raman spectroscopy, we used the CRM 200 (WiTec, Germany) with 100× lens (Olympus, N. A. 0.9) and ~1 mW of 532 nm laser. Polarization direction was checked by GX-AN360 (Olympus) filter. AFM images were taken by SPA400 (SEIKO, Japan) and JEOL7100F and JEOL7600F was used for SEM images. Tapping mode was used for obtaining morphology of the samples.

■ ASSOCIATED CONTENT

Supporting Information. Additional information and figures. This material is available free of charge via the Internet at http://pubs.acs.org.

■ AUTHOR INFORMATION

Corresponding Author
*E-mail: leeyoung@skku.edu.

■ ACKNOWLEDGMENT

This study was supported by the STAR-faculty program (2010-0029653) and WCU (World Class University) program (R31-2008-10029), the International Research & Development Program (2010-00429) of the NRF funded by the MEST of Korea.

■ REFERENCES

(1) Chae, S. J.; Güneş, F.; Kim, K. K.; Kim, E. S.; Han, G. H.; Kim., S. M.; Shin., H.; Yoon, S.; Choi, J; Park, M. H.; Yang, C. W.; Pribat, D.; Lee, Y. H. *Adv. Mater.* **2009**, *21*, 2328.

(2) Reina, A.; Jia, X.; Ho, J.; Nezich, D.; Son, H.; Bulovic, V.; Dresselhaus, M. S.; Kong, J. *Nano Lett.* **2009**, *9*, 30.

(3) Kim, K. S.; Zhao, Y.; Jang, H; Lee, S. Y.; Kim, J. M.; Kim, K. S.; Ahn, J.; Kim, P.; Choi, J.; Hong, B. H. *Nature* **2009**, *457*, 706.

(4) Güneş, F.; Han, G. H.; Kim, K. K.; Kim, E. S.; Chae, S. J.; Park, M. H.; Jeong, H. K.; Lim, S. J.; Lee, Y. H. *Nano* **2009**, *4*, 83.

(5) Pollard, A. J.; Nair, R. R.; Sabki, S. N.; Staddon, C. R.; Perdigao, L. M. A.; Hsu, C. H.; Garfitt, J. M.; Gangopadhyay, S.; Gleeson, H. F.; Geim, A. K.; Beton, P. H. *J. Phys. Chem. C* **2009**, *113*, 16565.

(6) Miyata, Y.; Kamon, K.; Ohashi, K.; Kitaura, R.; Yoshimura, M.; Shinohara, H. *Appl. Phys. Lett.* **2010**, *96*, 263105.

(7) Li, X.; Cai, W.; An, J.; Kim, S.; Nah, J.; Yang, D.; Piner, R.; Velamakanni, A.; Jung, I.; Tutuc, E.; Banerjee, S. K.; Colombo, L.; Ruoff, R. S. *Science* **2009**, *324*, 1312.

(8) Li, X.; Cai, W.; Colombo, L.; Ruoff, R. S. *Nano Lett.* **2009**, *9*, 4268.

(9) Bhaviripudi, S.; Jia, X.; Dresselhaus, M. S.; Kong, J. *Nano Lett.* **2009**, *10*, 4128.

(10) Li, X.; Magnuson, C. W.; Venugopal, A.; An, J.; Suk, J. W.; Han, B.; Borysiak, M.; Cai, W.; Velamakanni, A.; Zhu, Y.; Fu, L.; Vogel, E. M.; Voelkl, E.; Colombo, L.; Ruoff, R. S. *Nano Lett.* **2010**, *10*, 4328.

(11) Gao, L.; Ren, W.; Zhao, J.; Ma, L.-P.; Chen, Z.; Cheng, H.-M. *Appl. Phys. Lett.* **2010**, *97*, 183109.

(12) Chen, J.-H.; Jang, C.; Xiao, S.; Ishigami, M.; Fuhrer, M. S. *Nat. Nanotechnology* **2008**, *3*, 206.

(13) Li, X.; Magnuson, C. W.; Venugopal, A.; Tromp, R. M.; Hannon, J. B.; Vogel, E. M.; Voelkl, E.; Colombo, L.; Ruoff, R. S. *J. Am. Chem. Soc.* **2011**, *133*, 2816.

(14) Yu, Q.; Jauregui, L. A.; Wu, W.; Colby, R.; Tian, J.; Su, Z.; Cao, H.; Liu, Z.; Pandey, D.; Wei, D.; Chung, T. F.; Peng, P.; Guisinger, N. P.; Stach, E. A.; Bao, J.; Pei, S. -S.; Chen, Y. P. *Nat. Mater.* **2011**, *10*, 443.

(15) Mattevi, C.; Kim, H.; Chhowalla, M. *J. Mater. Chem.* **2011**, *21*, 3324.

(16) Baraton, L.; He, Z.; Lee, C. S.; Maurice, J.-L.; Cojocaru, C. S.; Gourgues-Lorenzon, A.-F.; Lee, Y. H.; Pribat, D. *Nanotechnology* **2011**, *22*, 085601.

(17) Huang, P. Y.; Ruiz-Vargas, C. S.; van der Zande, A. M.; Whitney, W. S.; Levendorf, M. P.; Kevek, J. W.; Garg, S.; Alden, J. S.; Hustedt, C. J.; Zhu, Y.; Park, J.; McEuen, P. L.; Muller, D. A. *Nature* **2011**, *469*, 389.

(18) Grüneis, A.; Saito, R.; Samsonidze, Ge. G.; Kimura, T.; Pimenta, M. A.; Jorio, A.; Souza Filho, A. G.; Dresselhaus, G.; Dresselhaus, M. S. *Phys. Rev. B* **2003**, *67*, 165402.

(19) Mafra, D. L.; Samsonidze, G.; Malard, L. M.; Elias, D. C.; Brant, J. C.; Plentz, F.; Alves, E. S.; Pimenta, M. A. *Phys. Rev. B* **2007**, *76*, 233407.

(20) Yoon, D.; Moon, H.; Son, Y.-W.; Samsonidze, G.; Park, B. H.; Kim, J. B.; Lee, Y. P.; Cheong, H. *Nano Lett.* **2008**, *8*, 4270.

(21) Krauss, B.; Lohmann, T.; Chae, D.-H.; Haluska, M.; von Klitzing, K.; Smet, J. H. *Phys. Rev. B* **2009**, *79*, 165428.

(22) Han, G. H.; Chae, S. J.; Kim, E. S.; Güneş, F.; Lee, I. H.; Lee, S. W.; Lee, S. Y.; Lim, S. C.; Jeong, H. K.; Jeong, M. S.; Lee, Y. H. *ACS Nano* **2011**, *5*, 263.

(23) Robertson, A. W.; Warner, J. H. *Nano Lett.* **2011**, *11*, 1182.